



Whole-genome and transcriptome profiling of a metastatic thyroid-like follicular renal cell carcinoma

Jenny J. Ko,¹ Jasleen K. Grewal,² Tony Ng,³ Jean-Michel Lavoie,⁴ My Linh Thibodeau,^{2,5,6} Yaoqing Shen,² Andrew J. Mungall,² Greg Taylor,² Kasmintan A. Schrader,⁶ Steven J.M. Jones,² Christian Kollmannsberger,⁴ Janessa Laskin,⁴ and Marco A. Marra²

¹Systemic Therapy, BC Cancer – Abbotsford, Abbotsford, British Columbia V2S 0C2, Canada; ²Canada's Michael Smith Genome Sciences Centre, Vancouver, British Columbia V5Z 4S6, Canada; ³Department of Pathology and Laboratory Medicine, Vancouver General Hospital, Vancouver, British Columbia V5Z 1M9, Canada; ⁴Systemic Therapy, BC Cancer – Vancouver, Vancouver, British Columbia V5Z 4E6, Canada; ⁵Department of Medical Genetics, University of British Columbia, Canada's Michael Smith Genome Sciences Centre, Vancouver, British Columbia V5Z 4S6, Canada; ⁶Hereditary Cancer Program, BC Cancer – Vancouver, Vancouver, British Columbia V5Z 4E6, Canada

Abstract Thyroid-like follicular renal cell carcinoma (TLFRCC) is a rare cancer with few reports of metastatic disease. Little is known regarding genomic characteristics and therapeutic targets. We present the clinical, pathologic, genomic, and transcriptomic analyses of a case of a 27-yr-old male with TLFRCC who presented initially with bone metastases of unknown primary. Genomic DNA from peripheral blood and metastatic tumor samples were sequenced. A transcriptome of 280 million sequence reads was generated from the same tumor sample. Tumor somatic expression profiles were analyzed to detect aberrant expression. Genomic and transcriptomic data sets were integrated to reveal dysregulation in pathways and identify potential therapeutic targets. Integrative genomic analysis with The Cancer Genome Atlas (TCGA) data set revealed the following outliers in gene expression profiles: *CDK6* (81st percentile), *MYC* (99th percentile), *AR* (100th percentile), *PDGFRA* and *PDGFRB* (99th and 100th percentiles, respectively), and *MAP2K2* (86th percentile). The patient received first-line sunitinib to target *PDGFRA* and *PDGFRB* and had stable disease for >6 mo, followed by nivolumab upon progression. To the authors' knowledge, this is the first reported case of comprehensive somatic genomic analyses in a patient with metastatic TLFRCC. Somatic analyses provided molecular confirmation of the primary site of cancer and potential therapeutic strategies in a rare disease with little evidence of efficacy on systemic therapy.

Corresponding author:
jenny.ko@bccancer.bc.ca

© 2018 Ko et al. This article is distributed under the terms of the Creative Commons Attribution-NonCommercial License, which permits reuse and redistribution, except for commercial purposes, provided that the original author and source are credited.

Ontology terms: malignant genitourinary tract tumor; renal neoplasm

Published by Cold Spring Harbor Laboratory Press

doi: 10.1101/mcs.a003137

[Supplemental material is available for this article.]

INTRODUCTION

Thyroid-like follicular renal cell carcinoma (TLFRCC) is a rare histopathological entity initially described in the literature in 2006 (Jung et al. 2006). Since then, several cases have been published (Dong et al. 2016), mostly describing well-circumscribed resected renal masses. In general, TLFRCC exhibits histology similar to thyroid follicular carcinoma, including PAX8 immunopositivity seen in both renal and thyroid tumor, although it is expected to be negative for thyroid immunohistochemical markers (e.g., TTF1, thyroglobulin). Few cases of metastatic TLFRCC have been described (Dhillon et al. 2011; Dong et al. 2016) and never,

to our knowledge, associated with integrative genomic analyses. We present a case of TLFRC diagnosis and tumor genome and whole transcriptome sequencing, as well as matched blood whole-genome analysis. Potentially relevant implications for systemic treatment are described.

RESULTS

Clinical Presentation and Family History

A 27-yr-old man with a previous history of bilateral congenital external rotation of the hip presented with gradual-onset right hip pain. A computed tomography (CT) scan of the right femur and hip revealed a well-corticated and ossified mass in the anterolateral aspect of the proximal femur, consistent with a well-healed previous avulsion injury. Subsequently, a follow-up magnetic resonance imaging (MRI) revealed another lesion not seen on initial CT scan involving the medial end of the right superior pubic ramus, 3.6 × 4.7 × 3.3 cm in size (Fig. 1A). A biopsy of the mass was obtained and showed findings suggestive of TLFRC (see Histologic Analysis below). CT of the chest, abdomen, and pelvis also showed a 3.6-cm simple cystic lesion at the interpolar region of the left kidney, with no other evidence of malignancy (Fig. 1B). No abnormality was found on thyroid ultrasound and subsequent radioactive iodine scan.

A positron-emission tomography (PET)/CT scan performed 6 wk after the initial CT scan revealed interval progression of the pubic ramus mass, now 6 × 4.5 cm and demonstrating fludeoxyglucose-18F (FDG) avidity. Additional FDG-avid bone lesions were noted at the right femoral neck, throughout the pelvis, 11th rib, manubrium and thoracic spine at the level of T6 and T10. The patient underwent a repeat core biopsy of the pubic ramus bony mass for genomic analysis. A biopsy of the left renal cyst was performed on the same occasion. The renal biopsy showed evidence of necrotic high-grade malignant cells consistent with sampling of a necrotic area within the tumor or possibly evidence of a regressed primary. Family history was remarkable for early-onset degenerative bone disease in his brother, adult-onset seizure disorder in his father, chronic lymphocytic leukemia in his paternal grandfather in his 70s, lung cancer in his maternal grandmother in her 70s, and breast cancer in his

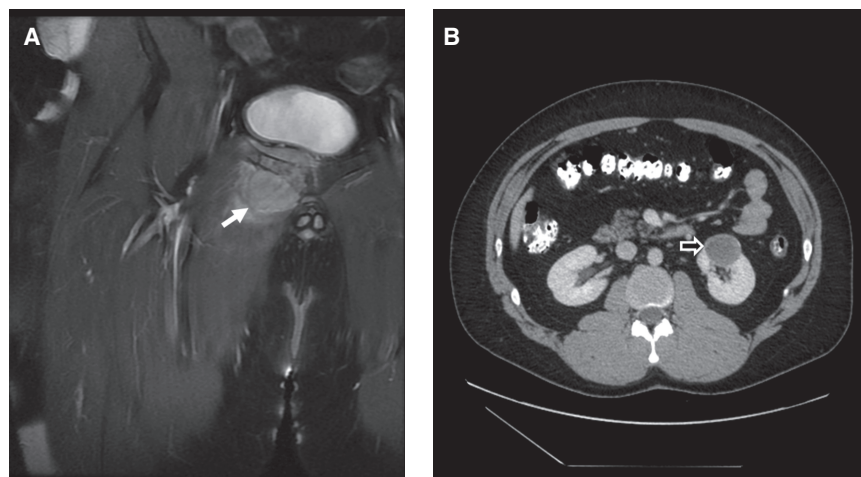


Figure 1. Radiologic studies of metastatic and primary lesions. (A) MRI of a pelvic lesion from which a biopsy was obtained (T2 postgadolinium; solid white arrow); (B) CT imaging of a renal cyst in the left kidney (axial abdomen/pelvic 3 mm; black arrow with white outline).

maternal great-grandmother. There was no family history of learning difficulties, congenital anomalies, recurrent miscarriages, or stillbirths.

Histologic Analysis

Core biopsies of the right pubic ramus mass were taken and revealed a moderately differentiated carcinoma comprised of cuboidal and hobnailed epithelial cells, and eosinophilic globules reminiscent of colloid were seen in some of the glandular spaces (Fig. 2A). No papillary architecture or clear cell morphology could be identified. Immunohistochemical stains were positive for CK20 (Fig. 2B), PAX8 (Fig. 2C), and P504S and negative for cytokeratin (CK) 7, thyroid transcription factor (TTF)-1, thyroglobulin, high-molecular weight CK (34 β E12), and CD10. Carbonic anhydrase IX immunohistochemistry showed very weak equivocal staining. The overall pattern was suggestive of TFRCC. Subsequent core biopsies of the left renal mass showed only necrotic tissue; however, these biopsies did show ghost outlines of a cellular proliferation that would be consistent with a primary renal malignancy (Fig. 2D). Given the histologic features and immunophenotype of the pubic ramus mass, and the absence of any other primary sites on clinical and radiologic workup, the final pathologic diagnosis was that of a metastatic carcinoma of renal cell origin.

Genomic Analyses

Tumor Whole-Genome and Transcriptome Sequencing

The pubic ramus bone biopsy was submitted for whole-genome and transcriptome sequencing. The Spearman correlation of the transcriptome against a background of cancers from The Cancer Genome Atlas (TCGA) average groups indicated that the cancer was similar to

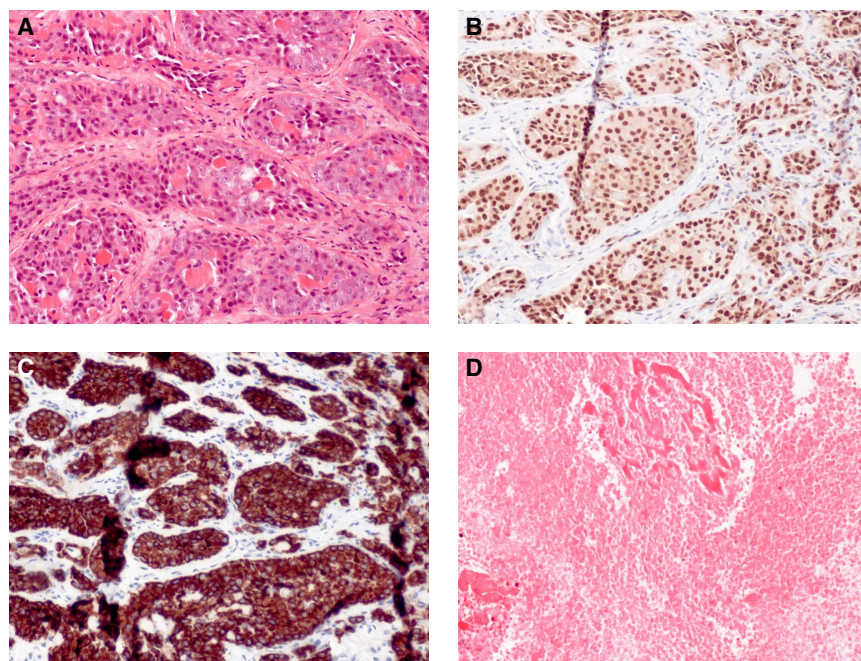


Figure 2. Histologic analysis of right pubic ramus mass and left renal mass. (A) Hematoxylin & eosin (H&E) staining of core biopsy of right pubic ramus mass (200 \times magnification). Immunohistochemistry of right pubic ramus mass for (B) CK20 and (C) PAX-8 (200 \times magnification). (D) H&E staining of core biopsy of left renal mass (200 \times magnification).

papillary renal cell carcinoma (pRCC). This observation was corroborated by genomic findings, as discussed below.

Single-Nucleotide Variants

Comparison of the genomic sequencing results from the tumor against the peripheral blood (normal) sample detected a total of 25 somatic nonsynonymous single nucleotide variants (SNVs) and two truncating insertion/deletion events (indels) within coding regions. This tumor displayed a moderate mutational burden compared to TCGA pRCC data set (The Cancer Genome Atlas Research Network et al. 2016), estimated at 26th percentile (SNVs) and 15th percentile (indels). The SNVs or indels identified were not of any known clinical, diagnostic, or biological relevance, based upon numerous SNV annotation databases, including OncoKB.org, FoundationOne.org, Cosmic, pct.mdanderson.org, My Cancer Genome, and Clarity Foundation. Six somatic variants of uncertain significance (VUSs) were detected in known cancer-related genes including *KRAS*, I187T; *CAT*, F185I; *CEP290*, Q284H; and *CSDE1*, D767N.

Structural Variants

A de novo assembly of the genome and transcriptome detected 92 structural variants (SVs) in which at least one breakpoint is within a gene. Among them, 16 SVs were expressed in the transcriptome as well. This places the SV burden of this tumor at the 68th percentile among our local pancancer database of 339 cases of diverse cancer types (Laskin et al. 2015). None of the SVs had any known biological or clinical significance.

Copy-Number Variants

A diploid model with an estimated 55% tumor content was inferred based on the read coverage ratio, prediction of allelic imbalance, and loss of heterozygosity (LOH) in the sample (see Methods). This ploidy model was used to estimate copy-number changes in the tumor genome. A single copy loss was detected for the tumor suppressor gene, *TP53*. No additional copy-number variants of interest were observed.

Transcriptome Analysis

A pairwise correlation analysis of the sample's transcriptome was undertaken to identify the closest correlated cancer type for the tumor from across approximately 40 different tumor types available from TCGA (see Methods) and in-house cohorts. The tumor sample correlated most strongly with kidney cancers, including clear cell renal cell carcinoma (ccRCC) and pRCC (KIRP) (Fig. 3A). Based on this observation, we further compared the sample against TCGA cancers using a more rigorous supervised machine learning comparator that used the entire transcriptome of the sample for a classification decision (see Methods). The comparator strongly indicated this to be similar to a kidney renal papillary carcinoma (Fig. 3B).

Based on the findings from the transcriptome-wide analysis, the genomic events and RNA-level enrichments were considered against a background of pRCC. A fold-change value for each gene was calculated against a normal kidney tissue transcriptome (see Methods), and a percentile rank of expression was calculated in comparison to the TCGA pRCC cohort. In the absence of any mutations of interest, expression outliers were identified and evaluated in conjunction with copy-number state and known biological function. Ten genes of interest were identified as having expression profiles that were outliers in the sample with respect to the TCGA pRCC data set (Table 1). Of particular interest among these genes were *CDK6* (81st percentile), *MYC* (99th percentile), *AR* (100th percentile), *PDGFRA* and *PDGFRB* (99th and 100th percentiles, respectively), and *MAP2K2* (86th percentile).

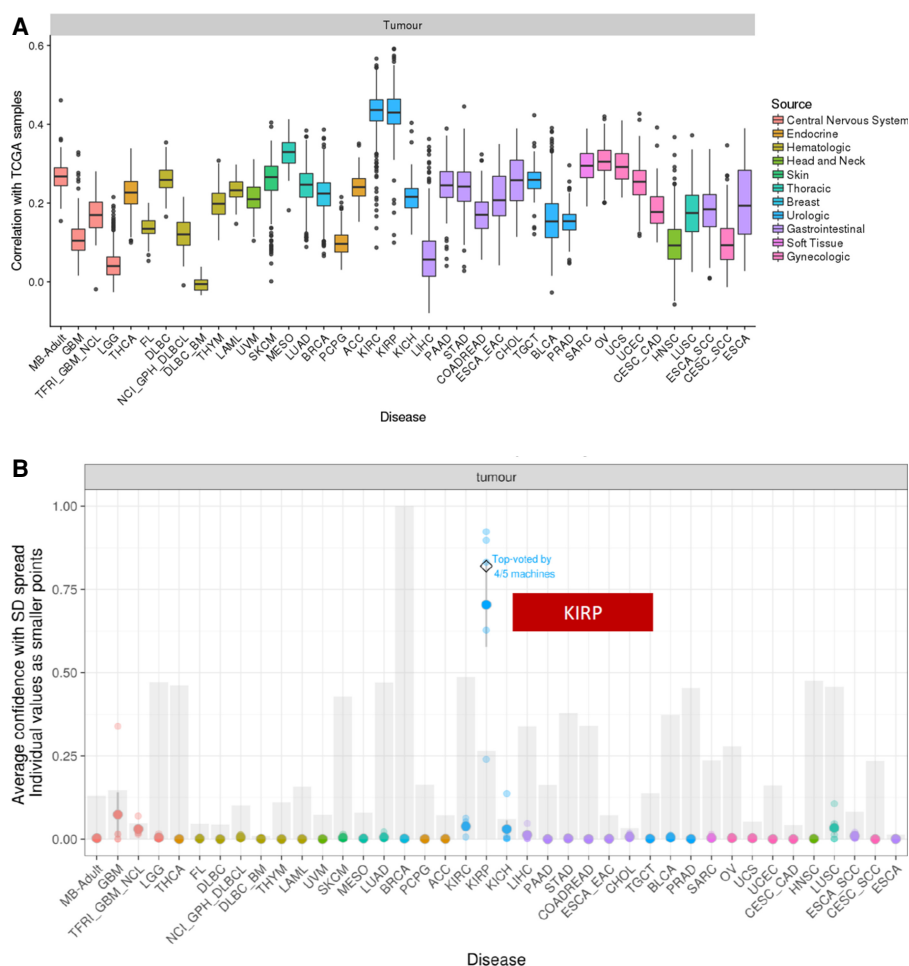


Figure 3. (A) Pairwise correlation analysis: comparison with TCGA cancer genome atlas. The cancer type with the highest median correlation to the input sample is indicated in red. (B) Supervised machine learning comparator that used the entire transcriptome of the sample for a classification decision. The cancer type with the highest predicted probability by the ensemble classifier is indicated in red. Gray bars indicate relative size of training cohorts, with breast cancer being the largest cohort of training samples for the classifier. All abbreviations follow the disease cohort codes used by the TCGA consortium (see Methods). (KIRP, pRCC) Kidney renal papillary cell carcinoma, (KIRC, ccRCC) kidney renal clear cell carcinoma.

Mutational Signatures

WGS mutational data were compared against previously cataloged mutational signatures (Alexandrov et al. 2013). The strongest signature was Signature 5, whose etiology is unknown, but has been shown to correlate with the age of patients at time of diagnosis (Alexandrov et al. 2013). It has been observed in all cancer types and most cancer samples, but the causality with cancer is uncertain.

Germline Genomic Analysis

Blood genome sequences were analyzed to detect germline mutations, copy-number changes, and SVs in 98 genes previously linked to hereditary cancer. No pathogenic or likely pathogenic SNVs, indels, or copy-number changes were identified in these genes.

Table 1. Genomic and transcriptomic findings

(a)					
Gene	Chr	Copy change (diploid model)	Copy type	TCGA pRCC percentile	Fold change versus kidney
<i>ERBB2</i>	17	+1 (HET)	Gain	1	1.06
<i>FHIT</i>	3	-1 (HOMD)	Hom Loss	6	-1.61
<i>MDM4</i>	1	+1 (HET)	Gain	88	-1.42
<i>TP53</i>	17	-1 (DLOH)	Deletion	25	1.42
(b)					
Gene	Chr	Copy change (diploid model)	Copy type	TCGA expression percentile ^a	Fold expression change ^b
<i>MAP3K14</i>	17	+1 (HET)	Gain	87	3.41
<i>COL1A1</i>	17	+1 (HET)	Gain	100	140.25
<i>ADGRA2</i>	8	-1 (DLOH)	Deletion	96	2.42
<i>CCNA2</i>	4	0 (HET)	Neutral	97	2.08
<i>CD274</i>	9	-1 (DLOH)	Deletion	97	3.57
<i>LMO1</i>	11	0 (HET)	Neutral	99	2.60
<i>MYC</i>	8	1 (HET)	Gain	99	13.54
<i>PRSS8</i>	16	0 (HET)	Neutral	1	-6.35
<i>PTEN</i>	10	0 (HET)	Neutral	0	-3.22
<i>RAD51</i>	15	0 (HET)	Neutral	90	2.02
<i>TOP2A</i>	17	1 (HET)	Gain	91	8.98
<i>CDK6</i>	7	0 (HET)	Neutral	81	1.36
<i>E2F1</i>	20	0 (HET)	Neutral	99	8.00
<i>E2F2</i>	1	-1 (DLOH)	Deletion	92	1.76
<i>E2F3</i>	6	0 (HET)	Neutral	99	1.11
<i>CTNBN1</i>	3	-1 (DLOH)	Deletion	84	-1.30
<i>BRD4</i>	19	0 (HET)	Neutral	99	2.03
<i>PDGFRA</i>	4	0 (HET)	Neutral	99	-3.12
<i>PDGFRB</i>	5	0 (HET)	Neutral	100	2.57
<i>MAP2K2</i>	19	0 (HET)	Neutral	86	2.68

In part (a), the key copy-number events are listed. In part (b), the key genes expressed differentially are listed, along with their corresponding copy-number states in the tumor genome. The expression percentile values (relative to TCGA pRCC tumors) and fold changes calculated from the respective RCCs, are also listed.

DLOH, deletion with loss of heterozygosity; HET, heterozygous; HOMD, homozygous deletion; Hom Loss, homozygous loss.

^aAs calculated against a background of TCGA kidney renal papillary carcinomas.

^bAs calculated against RPKM values from Illumina BodyMap 2.0 healthy kidney tissue.

Treatment Outcome

During this workup, the patient had further progression of the pelvic and spine lesions and a new lesion in the left orbit. He received palliative radiotherapy (40 Gy in 15 fractions) to all three sites. Decisions on systemic therapy were made based on clinical factors such as patient's performance status and availability of the medication, as well as recommendations from the provincial multidisciplinary genomic tumor board conference. Subsequently, sunitinib was initiated at 50 mg daily for 28 d followed by 14 d of treatment break. This was well tolerated and led to disease stability clinically and radiologically for 6 mo. At the time of progression, he received further radiotherapy and four cycles of nivolumab. There was no response to nivolumab, and he transitioned to best supportive care.

DISCUSSION

This case, to the authors' knowledge, is the first to report on comprehensive somatic genomic/transcriptomic analyses on a patient with TFRCC. With fewer than 30 cases described in literature to date, this diagnosis is often associated with young females who present with initially asymptomatic renal mass and with relatively few published cases of systemic metastasis (Amin et al. 2009; Dhillon et al. 2011; Lin et al. 2014; Wu et al. 2014; Nath et al. 2015; Chen et al. 2016; Muscara et al. 2017). Our case demonstrates a potentially aggressive and metastatic potential of TFRCC despite multiple courses of systemic and radiation therapy, unlike previously reported localized TFRCC cases that achieved long-term disease-free interval after resection of primary tumor. This case also marks the first detailed description of systemic therapies attempted for the treatment of a metastatic TFRCC.

Although not conclusive in isolation, our case lends some support to a possible role for genomic analysis in assisting the determination of primary site in cases in which the primary site is occult or unknown. Published cases show that genomic sequencing has utility in identifying what may histologically be classified as cancers of unknown origin (Handorf et al. 2013; Tothill et al. 2015). For example, two previously published cases with multiple metastases but without a clear renal primary tumor on imaging were independently found to be ccRCC through genome sequencing (Wei et al. 2015). Although both cases lacked *VHL* mutations, concurrent mutations in *PBRM1*, *SETD2*, and *TSC1* supported the diagnosis of RCC. In our patient's case, the radiologic and pathologic analyses were suspicious but not conclusive for TFRCC, because of the appearance of the renal mass resembling a simple cyst and histologic rarity. The data integration of genomic mutational profile and transcriptomic classification was used to help characterize the primary site of the tumor by providing comparison against a background of TCGA cancers. We also used these data to attempt to determine the subtype of RCC, although TCGA data set has coverage of only the three main subtypes of RCC (ccRCC, pRCC, and chromophobe RCC). This observation was later confirmed by pathology review of multiple biopsy specimens, which was consistent with TFRCC.

We note that the genomic analysis of our patient's TFRCC revealed no SNVs or indels with clinical, diagnostic, or biological relevance, whereas integrated concurrent transcriptomic sequencing revealed multiple potentially targetable pathways. In cases of rare histology subtypes, genomic analysis alone, especially when limited to exonic regions, may not identify potentially pathogenic or actionable downstream pathways.

In our patient's case, disease stability was achieved for a clinically meaningful time with sunitinib but not with nivolumab. Cytoplasmic expression of VEGF, VEGFR2, PDGF-B, and PDGFR- β in RCC tumor cells is different in various pathologic stages and cell types; VEGF and PDGF-B expression is reportedly higher in papillary than in ccRCC (Song et al. 2014). However, sunitinib likely exerts a complex multitarget effect on vascular endothelial growth factor-based proliferation across HIF1- α , VHL, PDGF, VEGF, VEGFR1, and VEGFR2; it is unclear whether PDGFR inhibition alone with another agent would have achieved disease stability or response (Dornbusch et al. 2013; Lai et al. 2018). Upon progression with sunitinib, an immune checkpoint inhibitor (ICI) with nivolumab was administered, but the patient did not derive benefit. Despite strong CD274 (PD-L1) expression (97th percentile), the patient's mutational burden was relatively modest. Currently, nivolumab is approved as standard-of-care second-line therapy in metastatic ccRCC, but its effect on other histologies of RCC is largely unknown (Motzer et al. 2015). In anecdotal cases and a small cohort study, it showed clinical benefit and a comparable response rate of 20% (Geynisman 2015; Koshkin et al. 2018). Expression of PD-L1 is not a reliable predictive marker of ICI efficacy in multiple tumor types including ccRCC (Motzer et al. 2015). Therefore, PD-L1 expression alone should not determine whether to try ICI as next-line therapy in treatment of mRCC.

The published literature shows one case report with no chromosomal aberration in TLFRC, in contrast to a trisomy of Chromosome 17 found in pRCC (Li et al. 2015). Another case of TLFRC showed monosomies in Chromosomes 7 and 17 (Dawane et al. 2015).

METHODS

Upon informed consent, a peripheral blood sample and metastatic tumor from the pelvis biopsy were submitted for genome library construction. To minimize library bias and coverage gaps associated with PCR amplification of high-GC or AT-rich regions, we have implemented a version of the TruSeq DNA PCR-free kit (E6875-6877B-GSC, New England Biolabs), automated on a Microlab NIMBUS liquid handling robot (Hamilton Robotics). Briefly, 500 ng of genomic DNA was arrayed in a 96-well microtiter plate and subjected to shearing by sonication (Covaris LE220). Sheared DNA was end-repaired and size-selected using paramagnetic PCRclean DX beads (C-1003-450, Aline Biosciences) targeting a 300- to 400-bp fraction. After 3' A-tailing, full length TruSeq adapters were ligated. Libraries were purified using paramagnetic (Aline Biosciences) beads. PCR-free genome library concentrations were quantified using a qPCR Library Quantification kit (KAPA, KK4824) prior to sequencing with paired-end 150-base reads on the Illumina HiSeqX platform using V4 chemistry according to manufacturer recommendations. The genome sequencing yielded a redundant sequence coverage depth of 37× and 81× for normal and tumor, respectively.

A transcriptome of 280 million sequence reads was also generated from the same tumor sample. Polyadenylated (poly(A)⁺) RNA was purified using the NEBNext Poly(A) mRNA Magnetic Isolation Module (E7490L, NEB) from 500 ng total RNA normalized in 35 μl for DNase I treatment (1 Unit, Invitrogen). DNase-treated RNA was purified using RNA MagClean DX beads (Aline Biosciences) on a Microlab NIMBUS liquid handler (Hamilton Robotics). Messenger RNA selection was performed using NEBNext Oligod(T)₂₅ beads (NEB) with incubation at 65°C for 5 min followed by snap-chilling at 4°C to denature RNA and facilitate binding of poly(A) mRNA to the beads. mRNA was eluted in 36 μl of Tris buffer.

First-strand cDNA was synthesized from the purified polyadenylated messenger RNA using the Maxima H Minus First Strand cDNA Synthesis kit (Thermo-Fisher) and random hexamer primers at a concentration of 5 μM along with a final concentration of 1 μg/μl Actinomycin D, followed by PCR Clean DX bead purification on a Microlab NIMBUS robot (Hamilton Robotics). The second-strand cDNA was synthesized following the NEBNext Ultra Directional Second Strand cDNA Synthesis protocol (NEB) that incorporates dUTP in the dNTP mix, allowing the second strand to be digested using USER enzyme (NEB) in the post-adaptor ligation reaction and thus achieving strand specificity.

cDNA was fragmented by Covaris LE220 sonication for 55 sec at a "Duty cycle" of 20% and "Intensity" of 5 to achieve 200- to 250-bp average fragment lengths. The paired-end sequencing library was prepared following the BC Cancer Genome Sciences Centre strand-specific, plate-based library construction protocol on a Microlab NIMBUS robot (Hamilton Robotics). Briefly, the sheared cDNA was subject to end repair and phosphorylation in a single reaction using an enzyme premix (NEB) containing T4 DNA polymerase, Klenow DNA Polymerase, and T4 polynucleotide kinase, incubated for 30 min at 20°C. Repaired cDNA was purified in 96-well format using PCR Clean DX beads (Aline Biosciences), and 3' A-tailed (adenylation) using Klenow fragment (3' to 5' exo minus) and incubation for 30 min at 37°C prior to enzyme heat inactivation. Illumina PE adapters were ligated for 15 min at 20°C. The adapter-ligated products were purified using PCR Clean DX beads, then digested with USER enzyme (1 U/μl, NEB) for 15 min at 37°C followed immediately by 13 cycles of indexed PCR using Phusion DNA Polymerase (Thermo Fisher Scientific Inc.) and Illumina's PE primer set. PCR parameters: for 1 min at 98°C followed by 13 cycles

of 15 sec at 98°C, 30 sec at 65°C, and 30 sec at 72°C, and then 5 min at 72°C. The PCR products were purified and size-selected using a 1:1 PCR Clean DX beads-to-sample ratio (twice), and the eluted DNA quality was assessed with Caliper LabChip GX for DNA samples using the High Sensitivity Assay (PerkinElmer Inc.) and quantified using a Quant-iT dsDNA High Sensitivity Assay Kit on a Qubit fluorometer (Invitrogen) prior to library pooling and size-corrected final molar concentration calculation for Illumina NextSeq500 sequencing with paired-end 75-base reads.

Somatic and germline genomic aberrations such as small mutations, copy-number alterations, and SVs were detected using a previously described pipeline (Jones et al. 2017; Thibodeau et al. 2018). Software components of the pipeline have in some cases been updated. BWA-mem (v0.7.6a) (Li and Durbin 2010) was used for aligning sequence reads to the reference human genome (hg19). Having sequenced both blood and tumor samples, variants identified from aligning the first sample were labeled as germline. The germline variants were subtracted from variants identified in the tumor sample, and the remaining variants were considered somatic. SAMtools (v0.1.17) (Li et al. 2009), MutationSeq (v4.3.5) (Ding et al. 2012), and Strelka (v1.0.6) (Saunders et al. 2012) were used to make the variant calls. Small insertions and deletions were identified using Strelka (v1.0.6) (Saunders et al. 2012) and Trans-AbySS (v1.4.10) (Birol et al. 2009; Simpson et al. 2009). AbySS (v1.3.4) (Robertson et al. 2010) was used to create de novo assemblies of genomic and transcriptomic data and Trans-AbySS (v1.4.10) identified large insertions, deletions, structural rearrangements, and fusions. Heterozygosity and regions of copy loss and gain were assessed using hidden Markov model-based approaches, CNaseq (v0.0.6) (Jones et al. 2010) and APOLLOH (v0.1.1) (Ha et al. 2012). Gene expression profile was used to generate Spearman correlation to all tumors from 37 tumor types from TCGA (<https://tcga-data.nci.nih.gov/tcga/>) and two in-house cohorts to infer tumor type. The TCGA cancer-type acronyms were adopted for encoding the tumor types of the expression cohorts and are detailed in Supplemental Table S1. These acronyms are also available from the Broad Institute's top level GDAC portal (<http://gdac.broadinstitute.org>). The supervised classifier was trained on TCGA primary cancers (Grewal JK, Tessier-Cloutier B, Jones SJM, et al., in prep.). Gene expression levels were calculated and compared to transcriptome sequencing data from the Illumina BodyMap (www.illumina.com; ArrayExpress ID: E-MTAB-513) and TCGA to detect aberrant expression. Genomic and transcriptomic data sets were integrated to reveal dysregulation in pathways and identify potential therapeutic targets.

ADDITIONAL INFORMATION

Data Deposition and Access

Genomic and transcriptomic data sets have been deposited at the European Genome-phenome Archive (EGA; <http://www.ebi.ac.uk/ega/> [January 27, 2018, date last accessed]) under accession number EGAD00001003722.

Ethics Statement

The study was approved by the University of British Columbia Research Ethics Board (REB# H12-00137 and H14-00681) and appropriate written informed consent was obtained from the patient for the study and publication before genomic and transcriptomic profiling.

Acknowledgments

We thank the patients and families who participated in this study. We also thank and acknowledge all of the researchers and clinicians who are not listed as authors but worked to make this

study possible. The results published here are in part based upon data generated by the following projects and obtained from dbGaP (<http://www.ncbi.nlm.nih.gov/gap>); The Cancer Genome Atlas managed by the NCI and NHGRI (<http://cancergenome.nih.gov>); and the Genotype-Tissue Expression (GTEx) Project, supported by the Common Fund of the Office of the Director of the National Institutes of Health (<https://commonfund.nih.gov/GTEx>).

Author Contributions

All authors were involved in the conception or design of the study or in analysis and interpretation of data and all were involved in drafting the article or in revising it critically for important intellectual content.

Funding

This research was generously funded through unrestricted philanthropic donations received through the BC Cancer Foundation. The POG study is supported by the BC Cancer Foundation and Genome British Columbia (project B20POG), Genome Canada and Genome BC, who contributed equipment and infrastructure (projects 202SEQ, 212SEQ, 12002), Canada Foundation for Innovation (projects 20070, 30198, 30981, 33408), and the BC Knowledge Development Fund. M.A.M. acknowledges infrastructure investments from the Canada Foundation for Innovation and the support of the Canada Research Chairs and CIHR Foundation (FDN-143288) programs (no grant numbers apply). Additionally, the Michael Smith Foundation for Health Research and the Canadian Institutes of Health Research funding held by K.A.S. supported this work, and J.-M.L. and M.L.T. are supported by the University of British Columbia Clinician Investigator Program.

Competing Interest Statement

The authors have declared no competing interest.

Received April 19, 2018;
 accepted in revised form
 September 12, 2018.

REFERENCES

- Alexandrov LB, Nik-Zainal S, Wedge DC, Aparicio SA, Behjati S, Biankin AV, Bignell GR, Bolli N, Borg A, Børresen-Dale AL, et al. 2013. Signatures of mutational processes in human cancer. *Nature* **500**: 415–421.
- Amin MB, Gupta R, Ondrej H, McKenney JK, Michal M, Young AN, Paner GP, Junker K, Epstein JI. 2009. Primary thyroid-like follicular carcinoma of the kidney: report of 6 cases of a histologically distinctive adult renal epithelial neoplasm. *Am J Surg Pathol* **33**: 393–400.
- Biroli I, Jackman SD, Nielsen CB, Qian JQ, Varhol R, Stazyk G, Morin RD, Zhao Y, Hirst M, Schein JE, et al. 2009. De novo transcriptome assembly with ABySS. *Bioinformatics* **25**: 2872–2877.
- Chen F, Wang Y, Wu X, Zhu Y, Jiang X, Chen S, Zhang Z, Zou Z, Yang Y, Zhu K, et al. 2016. Clinical characteristics and pathology of thyroid-like follicular carcinoma of the kidney: report of 3 cases and a literature review. *Mol Clin Oncol* **4**: 143–150.
- Dawane R, Grindstaff A, Parwani AV, Brock T, White WM, Nodit L. 2015. Thyroid-like follicular carcinoma of the kidney: one case report and review of the literature. *Am J Clin Pathol* **144**: 796–804.
- Dhillon J, Tannir NM, Matin SF, Tamboli P, Czerniak BA, Guo CC. 2011. Thyroid-like follicular carcinoma of the kidney with metastases to the lungs and retroperitoneal lymph nodes. *Hum Pathol* **42**: 146–150.
- Ding J, Bashashati A, Roth A, Oloumi A, Tse K, Zeng T, Haffari G, Hirst M, Marra MA, Condon A, et al. 2012. Feature-based classifiers for somatic mutation detection in tumour-normal paired sequencing data. *Bioinformatics* **28**: 167–175.
- Dong L, Huang J, Huang L, Shi O, Liu Q, Chen H, Xue W, Huang Y. 2016. Thyroid-like follicular carcinoma of the kidney in a patient with skull and meningeal metastasis: a unique case report and review of the literature. *Medicine (Baltimore)* **95**: e3314.
- Dornbusch J, Zacharis A, Meinhardt M, Erdmann K, Wolff I, Froehner M, Wirth MP, Zastrow S, Fuessel S. 2013. Analyses of potential predictive markers and survival data for a response to sunitinib in patients with metastatic renal cell carcinoma. *PLoS One* **8**: e76386.
- Geynisman DM. 2015. Anti-programmed cell death protein 1 (PD-1) antibody nivolumab leads to a dramatic and rapid response in papillary renal cell carcinoma with sarcomatoid and rhabdoid features. *Eur Urol* **68**: 912–914.

- Ha G, Roth A, Lai D, Bashashati A, Ding J, Goya R, Giuliany R, Rosner J, Oloumi A, Shumansky K, et al. 2012. Integrative analysis of genome-wide loss of heterozygosity and monoallelic expression at nucleotide resolution reveals disrupted pathways in triple-negative breast cancer. *Genome Res* **22**: 1995–2007.
- Handorf CR, Kulkarni A, Grenert JP, Weiss LM, Rogers WM, Kim OS, Monzon FA, Halks-Miller M, Anderson GG, Walker MG, et al. 2013. A multicenter study directly comparing the diagnostic accuracy of gene expression profiling and immunohistochemistry for primary site identification in metastatic tumors. *Am J Surg Pathol* **37**: 1067–1075.
- Jones SJ, Laskin J, Li YY, Griffith OL, An J, Bilenky M, Butterfield YS, Cezard T, Chuah E, Corbett R, et al. 2010. Evolution of an adenocarcinoma in response to selection by targeted kinase inhibitors. *Genome Biol* **11**: R82.
- Jones MR, Lim H, Shen Y, Pleasance E, Ch'ng C, Reisle C, Leelakumari S, Zhao C, Yip S, Ho J, et al. 2017. Successful targeting of the NRG1 pathway indicates novel treatment strategy for metastatic cancer. *Ann Oncol* **28**: 3092–3097.
- Jung SJ, Chung JI, Park SH, Ayala AG, Ro JY. 2006. Thyroid follicular carcinoma-like tumor of kidney: a case report with morphologic, immunohistochemical, and genetic analysis. *Am J Surg Pathol* **30**: 411–415.
- Koshkin VS, Barata PC, Zhang T, George DJ, Atkins MB, Kelly WJ, Vogelzang NJ, Pal SK, Hsu J, Appleman LJ, et al. 2018. Clinical activity of nivolumab in patients with non-clear cell renal cell carcinoma. *J Immunother Cancer* **6**: 9.
- Lai Y, Zhao Z, Zeng T, Liang X, Chen D, Duan X, Zeng G, Wu W. 2018. Crosstalk between VEGFR and other receptor tyrosine kinases for TKI therapy of metastatic renal cell carcinoma. *Cancer Cell Int* **18**: 31.
- Laskin J, Jones S, Aparicio S, Chia S, Ch'ng C, Deyell R, Eirew P, Fok A, Gelmon K, Ho C, et al. 2015. Lessons learned from the application of whole-genome analysis to the treatment of patients with advanced cancers. *Cold Spring Harb Mol Case Stud* **1**: a000570.
- Li H, Durbin R. 2010. Fast and accurate long-read alignment with Burrows–Wheeler transform. *Bioinformatics* **26**: 589–595.
- Li H, Handsaker B, Wysoker A, Fennell T, Ruan J, Homer N, Marth G, Abecasis G, Durbin R, Genome Project Data Processing Subgroup. 2009. The sequence alignment/map format and SAMtools. *Bioinformatics* **25**: 2078–2079.
- Li C, Dong H, Fu W, Qi M, Han B. 2015. Thyroid-like follicular carcinoma of the kidney and papillary renal cell carcinoma with thyroid-like feature: comparison of two cases and literature review. *Ann Clin Lab Sci* **45**: 707–712.
- Lin YZ, Wei Y, Xu N, Li XD, Xue XY, Zheng QS, Jiang T, Huang JB. 2014. Thyroid-like follicular carcinoma of the kidney: a report of two cases and literature review. *Oncol Lett* **7**: 1796–1802.
- Motzer RJ, Escudier B, McDermott DF, George S, Hammers HJ, Srinivas S, Tykodi SS, Sosman JA, Procopio G, Plimack ER, et al. 2015. Nivolumab versus everolimus in advanced renal-cell carcinoma. *N Engl J Med* **373**: 1803–1813.
- Muscara MJ, Simper NB, Gandia E. 2017. Thyroid-like follicular carcinoma of the kidney. *Int J Surg Pathol* **25**: 73–77.
- Nath V, Baliga M, Lewin J, Souza F, Akhtar I. 2015. Follicular thyroid carcinoma metastatic to the kidney: report of a case with cytohistologic correlation. *Case Rep Pathol* **2015**: 701413.
- Robertson G, Schein J, Chiu R, Corbett R, Field M, Jackman SD, Mungall K, Lee S, Okada HM, Qian JQ, et al. 2010. De novo assembly and analysis of RNA-seq data. *Nat Methods* **7**: 909–912.
- Saunders CT, Wong WS, Swamy S, Becq J, Murray LJ, Cheetham RK. 2012. Strelka: accurate somatic small-variant calling from sequenced tumor-normal sample pairs. *Bioinformatics* **28**: 1811–1817.
- Simpson JT, Wong K, Jackman SD, Schein JE, Jones SJ, Birol I. 2009. ABySS: a parallel assembler for short read sequence data. *Genome Res* **19**: 1117–1123.
- Song SH, Jeong IG, You D, Hong JH, Hong B, Song C, Jung WY, Cho YM, Ahn H, Kim CS. 2014. VEGF/VEGFR2 and PDGF-B/PDGFR- β expression in non-metastatic renal cell carcinoma: a retrospective study in 1,091 consecutive patients. *Int J Clin Exp Pathol* **7**: 7681–7689.
- The Cancer Genome Atlas Research Network, Linehan WM, Spellman PT, Ricketts CJ, Creighton CJ, Fei SS, Davis C, Wheeler DA, Murray BA, Schmidt L, et al. 2016. Comprehensive molecular characterization of papillary renal-cell carcinoma. *N Engl J Med* **374**: 135–145.
- Thibodeau ML, Bonakdar M, Zhao E, Mungall KL, Reisle C, Zhang W, Bye MH, Thiessen N, Bleile D, Mungall AJ, et al. 2018. Whole genome and whole transcriptome genomic profiling of a metastatic eccrine porocarcinoma. *NPJ Precis Oncol* **2**: 8.
- Tothill RW, Shi F, Paiman L, Bedo J, Kowalczyk A, Mileskshin L, Buela E, Klupacs R, Bowtell D, Byron K. 2015. Development and validation of a gene expression tumour classifier for cancer of unknown primary. *Pathology* **47**: 7–12.
- Wei EY, Chen YB, Hsieh JJ. 2015. Genomic characterisation of two cancers of unknown primary cases supports a kidney cancer origin. *BMJ Case Rep* **2015**: bcr2015212685.
- Wu WW, Chu JT, Nael A, Rezk SA, Romansky SG, Shane L. 2014. Thyroid-like follicular carcinoma of the kidney in a young patient with history of pediatric acute lymphoblastic leukemia. *Case Rep Pathol* **2014**: 313974.